



© 2021 Geological Society of America. For permission to copy, contact editing@geosociety.org

Manuscript received 23 October 2020 Revised manuscript received 29 March 2021 Manuscript accepted 1 April 2021

Published online 3 June 2021

# Highly localized upper mantle deformation during plate boundary initiation near the Alpine fault, New Zealand

Steven Kidder<sup>1,2</sup>, David J. Prior<sup>3</sup>, James M. Scott<sup>3</sup>, Hamid Soleymani<sup>2</sup> and Yilun Shao<sup>3</sup>

<sup>1</sup>Department of Earth and Atmospheric Sciences, City College of New York (CUNY), 160 Convent Avenue, New York, New York 10031, USA

<sup>2</sup>Department of Earth and Environmental Sciences, The Graduate Center, City University of New York, 365 5th Avenue, New York, New York 10016, USA

3Department of Geology, University of Otago, Leith Street Central, Dunedin 9054, New Zealand

#### **ABSTRACT**

Peridotite xenoliths entrained in magmas near the Alpine fault (New Zealand) provide the first direct evidence of deformation associated with the propagation of the Australian-Pacific plate boundary through the region at ca. 25–20 Ma. Two of 11 sampled xenolith localities contain fine-grained (40–150  $\mu m$ ) rocks, indicating that deformation in the upper mantle was focused in highly sheared zones. To constrain the nature and conditions of deformation, we combine a flow law with a model linking recrystallized fraction to strain. Temperatures calculated from this new approach (625–970  $^{\circ} C$ ) indicate that the observed deformation occurred at depths of 25–50 km. Calculated shear strains were between 1 and 100, which, given known plate offset rates (10–20 mm/yr) and an estimated interval during which deformation likely occurred (<1.8 m.y.), translate to a total shear zone width in the range 0.2–32 km. This narrow width and the position of mylonite-bearing localities amid mylonite-free sites suggest that early plate boundary deformation was distributed across at least ~60 km but localized in multiple fault strands. Such upper mantle deformation is best described by relatively rigid, plate-like domains separated by rapidly formed, narrow mylonite zones.

# INTRODUCTION

The width of plate boundary shear zones in Earth's mantle is a long-standing first-order question in geodynamics (e.g., Vauchez et al., 2012) and a poorly constrained boundary condition for models of major earthquakes and postseismic deformation (e.g., Bürgmann and Dresen, 2008). Teleseismic methods cannot resolve narrow shear zones (<~30 km) but commonly constrain—with poor depth resolution—wide (>100 km scale) zones of anisotropy beneath plate boundaries (e.g., Zietlow et al., 2014). Thus, it is unclear if continental strike-slip faults generally overlay wide deformation zones immediately beneath the Moho (e.g., Collins and Molnar, 2014) or if narrow shear zones penetrate the entire mantle lithosphere (e.g., Ford et al., 2014). Distinguishing between these possibilities using geologic evidence is difficult for a number of reasons, including (1) appropriate rock masses are rarely exposed, (2) microstructures formed during exhumation can be difficult to distinguish from those formed at deep levels, and (3) adequate barometers are commonly unavailable (e.g., Titus et al., 2007; Vauchez et al., 2012).

We describe a suite of mantle xenoliths from near New Zealand's Alpine fault (Fig. 1), an active continental transform fault (e.g., Norris and Toy, 2015). These xenoliths are unique in that (1) they sampled multiple locations (N=11) near the fault, (2) some samples are mylonites (highly sheared), and (3) their eruption coincided with the onset of plate boundary motion. We present a new approach that allows strain rate, deformation temperature, and shear zone width to be estimated from a xenolith "snapshot" of the critical, earliest moments of faulting.

## GEOLOGIC BACKGROUND

The Alpine fault comprises the  $\sim\!800$  km stretch of the Australia-Pacific plate boundary crossing New Zealand's South Island (e.g., Sutherland et al., 2000). Dextral strike-slip motion began at ca. 25–20 Ma following a period of extension and north-propagating rifting (Fig. 1; Sutherland et al., 2000). The mod-

ern transpressional period began at ca. 5–8 Ma (Batt et al., 2004). The trace of the Alpine fault coincides with preexisting structures that may have influenced its position (Sutherland et al., 2000; Lamb et al., 2016).

The studied spinel peridotite xenoliths occur in the Alpine dike swarm (Fig. 1), which also dates to ca. 25-20 Ma (Cooper, 2020). The xenoliths are mainly harzburgites and dunites (olivine Mg#  $[100 \times Mg/\{Mg + Fe\}]$  commonly >90; Scott et al., 2014; Liu et al., 2015). Some xenoliths contain minor hydrous phases (Scott et al., 2014), and calculated H<sub>2</sub>O concentrations in olivine are high ( $\sim$ 80 ppm; Li et al., 2018). Two-pyroxene thermometry on coarse-grained samples indicates peak or retrograde temperatures ranging from 800 to 1200 °C (Scott et al., 2014, 2016). These temperatures may pre-date deformation, but deformation temperatures are bracketed by these values and lower crustal temperatures of 600-700 °C at the onset of Alpine fault deformation (Vry et al., 2004; Briggs and Cottle, 2018; Kidder et al., 2018). The xenolith source depth exceeded ~25 km based on constraints on paleo-Moho depth (Lamb et al., 2015).

#### **MICROSTRUCTURES**

The peridotite xenoliths can be sorted into coarse- and fine-grained types (Fig. 2). Coarse-grained xenoliths (Fig. 2A) make up  $\sim\!\!90\%$  of 84 observed samples and occur at all the localities. Coarse-grained xenoliths are dominated by millimeter- to centimeter-scale grains, with grains of size 300–600  $\mu m$  also found in some samples along grain boundaries.

Fine-grained xenoliths were found at two localities: the 25–20 Ma Moeraki River valley and the 23.3  $\pm$  0.1 Ma Lake Wanaka diatreme (Fig. 1; Cooper, 2020). Fine-grained peridotites

CITATION: Kidder, S., et al., 2021, Highly localized upper mantle deformation during plate boundary initiation near the Alpine fault, New Zealand: Geology, v. 49, p. 1102–1106, https://doi.org/10.1130/G48532.1

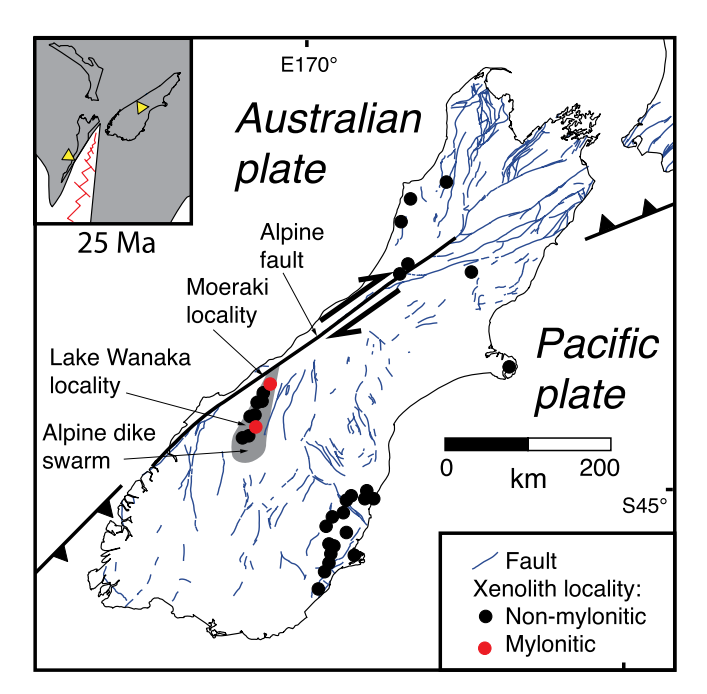


Figure 1. Map of New Zealand's South Island showing features described in the text. Inset shows the location's configuration at 25 Ma (Lamb et al., 2016) with continental crust shaded. The Alpine fault propagated northward from the tip of the Paleogene rift shown in red in the inset, connecting two points marked as yellow triangles. GPS coordinates of sample locations are provided by Scott (2020).

are absent at all 64 other known New Zealand xenolith localities (Fig. 1; Scott, 2020). The fine-grained Lake Wanaka xenoliths are mylonitic and layered and comprise a roughly 50:50 mixture of (1) large, millimeter-scale grains ("relicts") with aspect ratios as high as 10:1, and (2) zones of fine (40–150  $\mu$ m) recrystallized grains (grains formed during deformation) made up of olivine or orthopyroxene or mixtures of the two (Fig. 2B). Olivine relicts contain subgrains and undulose extinction. The fine-grained xenoliths at the Moeraki locality are unlayered and comprise a variably proportioned mixture of relicts and pure olivine matrix that also averages 50:50; i.e., overall recrystallized fraction of  $\sim$ 50%. The matrix grains in these samples have a size of 100-200 µm and

their boundaries tend to be straight or gently curved and commonly intersect at 120° triple junctions (Fig. 2C).

#### TIMING OF GRAIN SIZE REDUCTION

The microstructures of the fine-grained xenoliths are typical of highly deformed rocks from shear zones and deformation experiments (e.g., Warren and Hirth, 2006; Cross and Skemer, 2017). Fine-grained areas of such rocks composed of a single phase (e.g., lower part Fig. 2B; Fig. 2C) are energetically unstable and experience grain growth following deformation (e.g., Karato, 1989; Kidder et al., 2016). Using either the wet or dry grain growth equations from Karato (1989) at temperatures of 600–1200 °C and any initial grain size, we calculate

that the observed grains (Fig. 2C) would have increased beyond 150 µm if formed more than  $\sim$ 20,000 yr before entrainment. This calculation suggests that the mylonites are not inherited features pre-dating the Alpine fault but instead capture active deformation at the time of entrainment. We note that while the grain growth relationships of Karato (1989) are widely used, they may predict faster growth rates than occur in natural samples (e.g., Speciale et al., 2020). However, both in New Zealand and globally, xenolith localities containing fine-grained spinel peridotite are extremely rare (n = 7) and unique to active tectonic areas (Vauchez et al., 2012). We infer that the occurrence of mylonitic xenoliths near the Alpine fault at the moment of its formation is not coincidental but that the xenoliths are representative of the mantle at 25–20 Ma.

# DEFORMATION TEMPERATURE AND STRAIN

To constrain conditions of deformation recorded in the xenoliths, we apply a new technique combining three relationships: (1) a paleopiezometer based on experiments that link recrystallized grain size to differential stress (referred to as "stress" throughout); (2) a flow law that yields strain rate as a function of stress and temperature; and (3) a relationship between finite strain ("strain" hereafter) and recrystallized fraction (percentage of recrystallized grains versus relicts; Cross and Skemer, 2019). Alpine fault history provides a key additional constraint: the earliest likely onset of deformation at ca. 25 Ma and entrainment of mylonites at ca.  $23.3 \pm 0.1$  Ma are separated by < 1.8 m.y. Thus, multiplying strain rates from the flow law by 1.8 m.y. constrains total strain accommodated by the xenoliths. Relationships 2 and 3 can both plot on a graph of temperature versus strain (Fig. 3), with their intersection

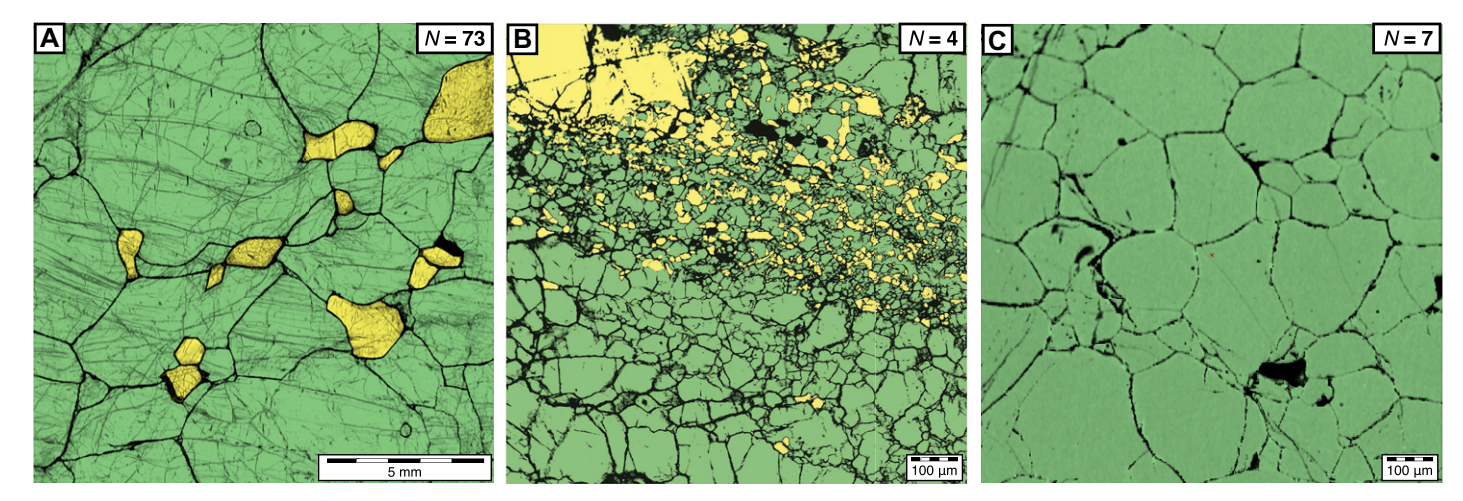


Figure 2. Micrographs of three xenolith types highlighting phase (olivine is false-colored green, pyroxene is yellow) and grain boundaries (darkened). "N" indicates numbers of each sample type. Note that the scale in A is 15× that of B and C. (A) Coarse-grained sample (MOE18). (B) Fine-grained mylonite sample (LWA10) containing a mixture of olivine and pyroxene. (C) Fine-grained unlayered sample (MOE 12) showing several 120° triple junctions.

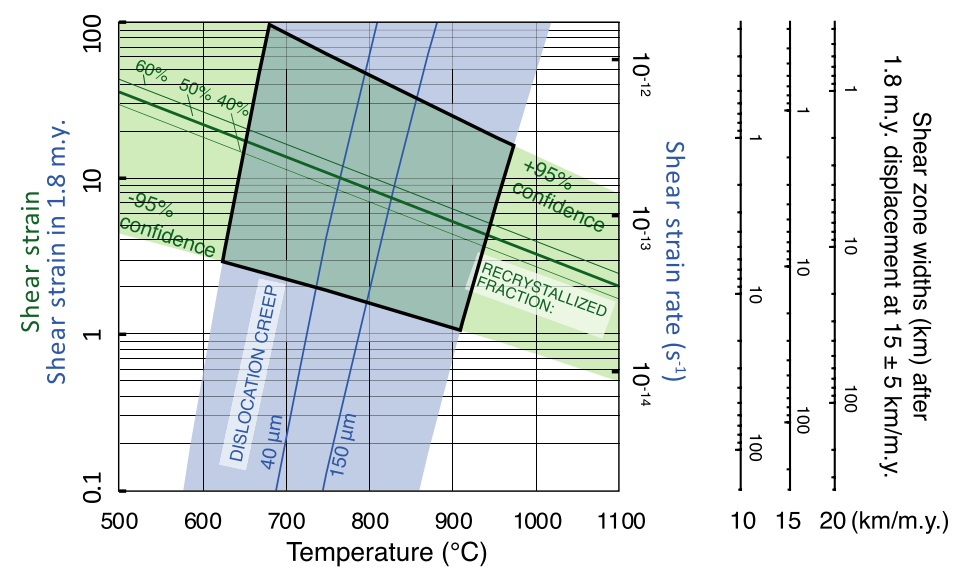


Figure 3. Relationships 2 and 3 plotted on a graph of temperature versus strain. Black-outlined area shows calculated deformation temperature, strain, and shear zone width based on the intersection of wet dislocation creep flow law (blue) and recrystallization relationship (green). Flow law (blue area) uses recrystallized grain sizes from fine-grained xenoliths (40–150  $\mu m$ ) and uncertainties in flow law and piezometer formulations. Shear strains were calculated from flow law–derived axial strain rates by multiplying by: (1) 1.8 m.y. over which deformation occurred, and (2) $\sqrt{3}$  (to convert axial to shear strain rate). Variations in recrystallization relationship due to variable recrystallized fraction (40%–60%) are shown to be relatively small. Alternative scales for shear zone width correspond to plausible 25 Ma Alpine fault offset rates of 10–20 km/m.y. (Sutherland et al., 2000).

constraining the temperature, strain, and strain rate of a plate boundary shear zone in the mantle within 1.8 m.y. of its initiation.

#### Relationship 1: Paleopiezometer

Recrystallized grain size is inversely proportional to stress (e.g., Twiss, 1977). To bracket reasonable stresses, we employed the olivine piezometer of Van der Wal et al. (1993) using recrystallized grain sizes from the coarsest and finest observed zones: a 150 µm grain size of a region that likely experienced post-deformation grain growth (e.g., Fig. 2C) corresponds to a stress of 21<sup>+6</sup> MPa; a 40 µm grain size (e.g., Fig. 2B) provides a stress of  $57^{+21}_{-13}$  MPa. The higher stress value is a maximum constraint because it comes from a phased-mixed zone (e.g., Fig. 2B); such zones are routinely finer grained than coexisting pure-phase regions (e.g., Cross and Skemer, 2017). We used a stereologic correction factor of 1.75 in these calculations (Van der Wal et al., 1993).

## **Relationship 2: Viscous Flow Law**

Using the stresses from the piezometer, we calculated strain rates as a function of temperature using the wet dislocation creep flow law for olivine (Fig. 3; Hirth and Kohlstedt, 2003). This flow law was chosen based on the evidence of wet conditions and microstructures indicative of dislocation activity in the mylonites. The other common deformation mechanism involving dislocations (dislocation-accommodated grain boundary sliding [disGBS]; e.g., Warren and

Hirth, 2006) is slower than dislocation creep at the conditions in Figure 3 (Hansen et al., 2011).

# Relationship 3: From Recrystallized Fraction to Finite Strain

Cross and Skemer (2019) demonstrated that recrystallized fraction is a largely material-independent function of strain and homologous temperature (the fraction of the material melt temperature). To plot this relationship for the xenoliths and estimate uncertainties (Fig. 3), we used the Cross and Skemer (2019) database to fit a new curve with the *Polyfit* function in Matlab (https://www.mathworks.com/help/matlab/ref/polyfit.html; see the Supplemental Material¹) using only samples containing similar recrystallized fractions as the xenoliths (50%  $\pm$  10% recrystallized).

The intersection of relationships 2 and 3 in Figure 3 indicates deformation temperatures in the range 625–970 °C and shear strains of 1–100. If deformation began more recently than 25 Ma (i.e., an interval shorter than 1.8 m.y. between deformation and entrainment), then the plotted flow-law lines would shift slightly to the right; e.g., an order of magnitude shorter time causes a +50° change in temperature.

# DISCUSSION

## **Narrow Upper Mantle Shear Zones**

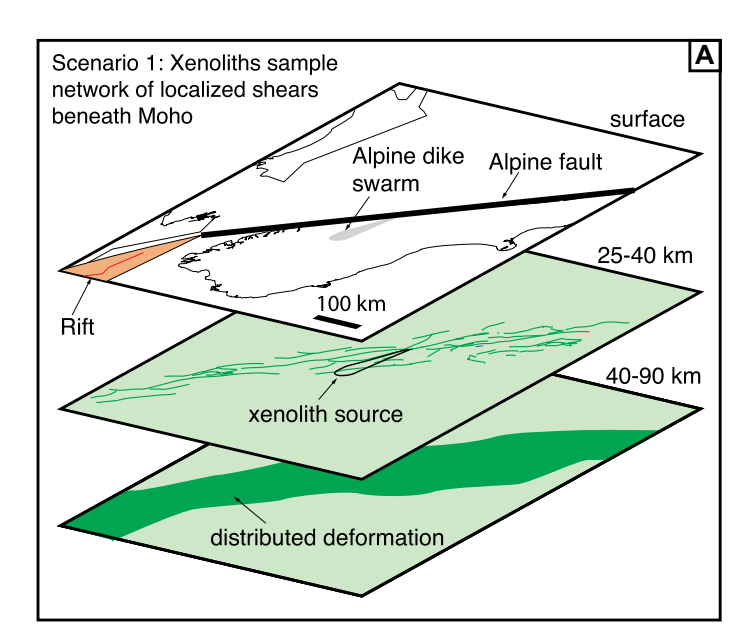
When combined with an estimated  $\sim 20$  °C/km paleo-geothermal gradient (Scott et al., 2014), the calculated deformation temperatures indicate a depth of no more than 50 km. Oligocene–Miocene crustal thickness is estimated at  $\sim 25$  km (Lamb et al., 2016), thus the mylonites formed in the uppermost mantle (25–50 km).

Mantle shear zone widths can be estimated if strains in the xenoliths (Fig. 3) are representative of a strike-slip shear zone deformed at 10–20 km/m.y. (Sutherland et al., 2000) for 1.8 m.y. For shear strains of 1–100, calculated widths are 0.2–32 km (Fig. 3). If the interval between the initiation of deformation and xenolith entrainment was shorter, estimated widths are reduced, e.g., a time interval of 0.2 m.y. results in widths of 0.02–3 km (see the Supplemental Material for examples).

The upper mantle within 60 km horizontal distance of the fault (or perhaps  $\sim 30\%$ –40% larger given likely Neogene crustal shortening; e.g., Little et al., 2002) was thus characterized by at least two narrow shear zones within minimally deformed wall rock. This interpretation is supported by four observations. First, the region affected by mylonitization (>120 km, assuming symmetry across the fault) is one or two orders of magnitude larger than the calculated shear zone widths. Second, several sites with exclusively coarse-grained xenoliths lie between sites containing evidence of mylonitization (Fig. 1). Third, a locality displaying exclusively coarsegrained xenoliths is found  $\sim 10$  km distant from the fault (Fig. 1). Thus, from geometric arguments alone, if a highly localized main fault strand was centered over the present-day surface expression of the fault, its width was <20 km. Fourth, fine-grained, mixed-phase shear zones (e.g., Fig. 2B) are generally dominated by diffusion creep rather than dislocation creep, making the above strain rate estimates minima and estimated shear zone widths an upper bound (e.g., Cross and Skemer, 2017; Mulyukova and Bercovici, 2019).

These observations are consistent with multiple, highly localized upper mantle fault strands running sub-parallel to the early Alpine fault trend in a region  $\sim$ 150 km wide (Fig. 4A). Such an array may have linked to more-distributed deformation at depth; e.g., Collins and Molnar (2014) interpreted from Pn wave anisotropy a modern 100-200-km-wide zone of penetrative deformation at depths of 40-60 km. Alternatively, the Alpine dike swarm may have intruded along a lithosphere-scale Riedel shear zone (e.g., Cooper, 2020), and the xenoliths could thus preserve deformation associated with this structure (Fig. 4B). Either way, these rocks indicate that upper mantle deformation associated with the early Australian-Pacific plate boundary was highly localized.

<sup>&</sup>lt;sup>1</sup>Supplemental Material. Supplemental figures, data, and code related to shear zone width estimates. Please visit https://doi.org/10.1130/GEOL.S.14605269 to access the supplemental material, and contact editing@geosociety.org with any questions.



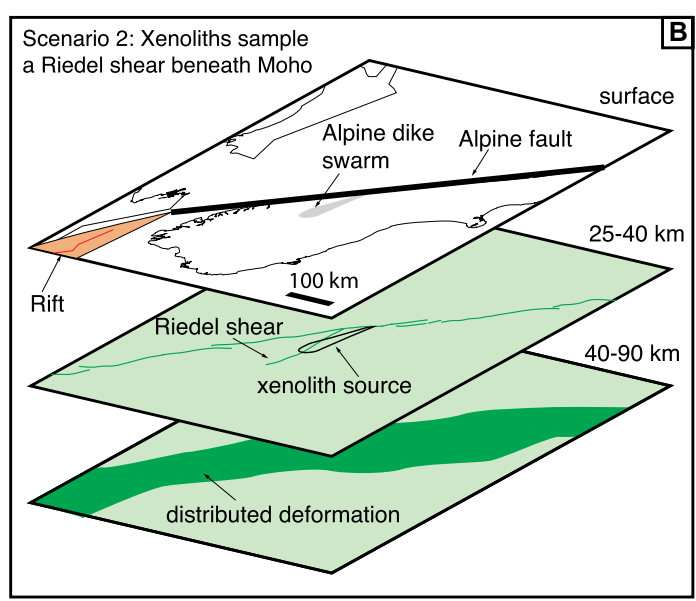


Figure 4. Cartoon showing two scenarios consistent with highly localized deformation in sub-Moho mantle lithosphere at ca. 23 Ma. The upper crust (white) is the same in both panels and is based on reconstructed paleogeography (Fig. 1 inset). Mantle is shown in green. Distributed deformation in the deep lithospheric mantle (40–90 km) is based on modern-day seismic anisotropy (e.g., Collins and Molnar, 2014). (A) Scenario 1: xenoliths sample an ~150-km-wide, Alpine fault-parallel, heterogeneous zone containing both localized shear zones and coarse-grained rocks relatively unaffected by shearing. (B) Scenario 2: xenoliths sample an isolated fault splay (Riedel shear).

## **Relevance to Modern Strike-Slip Faults**

Seismic anisotropy occurs at poorly constrained depths in the present-day mantle beneath the modern Alpine fault, with a fast direction oriented within  $5^{\circ}$ – $25^{\circ}$  of strike (e.g., Collins and Molnar, 2014; Zietlow et al., 2014). Such anisotropy results from the preferred orientation of olivine crystals in zones wider than  $\sim$ 50 km (e.g., Vauchez et al., 2012; Skemer and Hansen, 2016). Thus, mylonite zones such as those sampled are too narrow to affect seismic anisotropy.

The modern degree of mantle localization may also differ from that recorded in the xenoliths due to crustal thickening and extensive deformation since 25 Ma, but if a narrow shear zone persisted, it could explain the sharp change in lithospheric thickness across the Alpine fault (Hua et al., 2018).

In terms of Moho depth and rates of plate motion, the 25–20 Ma Alpine fault was similar to the modern San Andreas fault (California, USA; e.g., Ford et al., 2014). Mylonites are not present at the single known xenolith locality adjacent to the San Andreas fault (Titus et al., 2007). The absence of mylonites at one locality should not be considered evidence against a highly localized shear zone, however: for the early Alpine fault example, only 18% of localities contain mylonites. It appears most likely that a single xenolith locality would not sample a highly localized shear zone.

#### CONCLUSIONS

The xenoliths provide rare samples of an initiating continental transform fault at mantle depths and the earliest-known physical evidence

of Alpine fault deformation. Within  $\sim 1.8$  m.y. of likely fault initiation, mantle deformation was focused in narrow, highly localized shear zones with a total width of 0.2–32 km. These findings support the view that the upper mantle lithosphere consists of relatively rigid, plate-like domains separated by rapidly developed zones of focused deformation (Bercovici and Ricard, 2014; Ford et al., 2014).

#### ACKNOWLEDGMENTS

This work was funded by U.S. National Science Foundation grants EAR-1524602 and EAR-1951142 to S. Kidder; a "Tectonics of Zealandia" GNS Science (New Zealand) subcontract to D. Prior and Y. Shao; and New Zealand Foundation for Research, Science and Technology contract UOX1004 to J. Scott. We thank D. Bercovici and two anonymous reviewers, L. Mameri, and editor G. Dickens for comments on earlier versions of the manuscript, A. Cross for Matlab code, and A. Cooper for Moeraki samples.

#### REFERENCES CITED

Batt, G.E., Baldwin, S.L., Cottam, M.A., Fitzgerald, P.G., and Brandon, M.T., 2004, Cenozoic plate boundary evolution in the South Island of New Zealand: New thermochronological constraints: Tectonics, v. 23, TC4001, https://doi .org/10.1029/2003TC001527.

Bercovici, D., and Ricard, Y., 2014, Plate tectonics, damage, and inheritance: Nature, v. 508, p. 513–516, https://doi.org/10.1038/nature13072.

Briggs, S.I., and Cottle, J.M., 2018, Accessory mineral petrochronology reveals 30 m.y. of partial melting during the separation of Zealandia from eastern Gondwana: Lithosphere, v. 11, p. 169–189, https://doi.org/10.1130/L1021.1.

Bürgmann, R., and Dresen, G., 2008, Rheology of the lower crust and upper mantle: Evidence from rock mechanics, geodesy, and field observations: Annual Review of Earth and Planetary Sciences, v. 36, p. 531–567, https://doi.org/10.1146/ annurev.earth.36.031207.124326. Collins, J.A., and Molnar, P., 2014, Pn anisotropy beneath the South Island of New Zealand and implications for distributed deformation in continental lithosphere: Journal of Geophysical Research: Solid Earth, v. 119, p. 7745–7767, https://doi.org/10.1002/2014JB011233.

Cooper, A.F., 2020, Petrology and petrogenesis of an intraplate alkaline lamprophyre-phonolite-carbonatite association in the Alpine Dyke Swarm, New Zealand: New Zealand Journal of Geology and Geophysics, v. 63, p. 469–488, https://doi.org/10.1080/00288306.2019.1684324.

Cross, A.J., and Skemer, P., 2017, Ultramylonite generation via phase mixing in high-strain experiments: Journal of Geophysical Research: Solid Earth, v. 122, p. 1744–1759, https://doi.org/10.1002/2016JB013801.

Cross, A.J., and Skemer, P., 2019, Rates of dynamic recrystallization in geologic materials: Journal of Geophysical Research: Solid Earth, v. 124, p. 1324–1342, https://doi.org/10.1029/2018JB016201.

Ford, H.A., Fischer, K.M., and Lekic, V., 2014, Localized shear in the deep lithosphere beneath the San Andreas fault system: Geology, v. 42, p. 295–298, https://doi.org/10.1130/G35128.1.

Hansen, L.N., Zimmerman, M.E., and Kohlstedt, D.L., 2011, Grain boundary sliding in San Carlos olivine: Flow law parameters and crystallographic-preferred orientation: Journal of Geophysical Research, v. 116, B08201, https:// doi.org/10.1029/2011JB008220.

Hirth, G., and Kohlstedt, D., 2003, Rheology of the upper mantle and the mantle wedge: A view from the experimentalists, *in* Eiler, J., ed., Inside the Subduction Factory: American Geophysical Union Geophysical Monograph 138, p. 83–105, https://doi.org/10.1029/138GM06.

Hua, J., Fischer, K.M., and Savage, M.K., 2018, The lithosphere-asthenosphere boundary beneath the South Island of New Zealand: Earth and Planetary Science Letters, v. 484, p. 92–102, https:// doi.org/10.1016/j.epsl.2017.12.011.

Karato, S., 1989, Grain growth kinetics in olivine aggregates: Tectonophysics, v. 168, p. 255–273, https://doi.org/10.1016/0040-1951(89)90221-7.

- Kidder, S., Hirth, G., Avouac, J.-P., and Behr, W., 2016, The influence of stress history on the grain size and microstructure of experimentally deformed quartzite: Journal of Structural Geology, v. 83, p. 194–206, https://doi.org/10.1016/ j.jsg.2015.12.004.
- Kidder, S.B., Toy, V.G., Prior, D.J., Little, T.A., Khan, A., and MacRae, C., 2018, Constraints on Alpine Fault (New Zealand) mylonitization temperatures and geothermal gradient from Ti-in-quartz thermobarometry: Solid Earth, v. 9, p. 1123–1139, https://doi.org/10.5194/se-9-1123-2018.
- Lamb, S., Smith, E., Stern, T., and Warren-Smith, E., 2015, Continent-scale strike-slip on a low-angle fault beneath New Zealand's Southern Alps: Implications for crustal thickening in oblique collision zones: Geochemistry Geophysics Geosystems, v. 16, p. 3076–3096, https://doi.org/10.1002/2015GC005990.
- Lamb, S., Mortimer, N., Smith, E., and Turner, G., 2016, Focusing of relative plate motion at a continental transform fault: Cenozoic dextral displacement >700 km on New Zealand's Alpine Fault, reversing >225 km of Late Cretaceous sinistral motion: Geochemistry Geophysics Geosystems, v. 17, p. 1197–1213, https://doi .org/10.1002/2015GC006225.
- Li, P., Scott, J.M., Liu, J., and Xia, Q.-k., 2018, Lateral H<sub>2</sub>O variation in the Zealandia lithospheric mantle controls orogen width: Earth and Planetary Science Letters, v. 502, p. 200–209, https://doi.org/10.1016/j.epsl.2018.09.004.
- Little, T.A., Holcombe, R.J., and Ilg, B.R., 2002, Kinematics of oblique collision and ramping inferred from microstructures and strain in middle crustal rocks, central Southern Alps, New Zealand: Journal of Structural Geology, v. 24, p. 219–239, https://doi.org/10.1016/S0191-8141(01)00060-8.
- Liu, J., Scott, J.M., Martin, C.E., and Pearson, D.G., 2015, The longevity of Archean mantle residues in the convecting upper mantle and their role in young continent formation: Earth and Planetary Science Letters, v. 424, p. 109–118, https://doi.org/10.1016/j.epsl.2015.05.027.

- Mulyukova, E., and Bercovici, D., 2019, A theoretical model for the evolution of microstructure in lithospheric shear zones: Geophysical Journal International, v. 216, p. 803–819, https://doi.org/10.1093/gji/ggy467.
- Norris, R.J., and Toy, V.G., 2015, Continental transforms: A view from the Alpine Fault: Journal of Structural Geology, v. 64, p. 3–31, https://doi.org/10.1016/j.jsg.2014.03.003.
- Scott, J.M., 2020, An updated catalogue of New Zealand's mantle peridotite and serpentinite: New Zealand Journal of Geology and Geophysics, v. 63, p. 428–449, https://doi.org/10.1080/0028 8306.2020.1776738.
- Scott, J.M., Waight, T.E., van der Meer, Q.H.A., Palin, J.M., Cooper, A.F., and Münker, C., 2014, Metasomatized ancient lithospheric mantle beneath the young Zealandia microcontinent and its role in HIMU-like intraplate magmatism: Geochemistry Geophysics Geosystems, v. 15, p. 3477–3501, https://doi.org/10.1002/2014GC005300.
- Scott, J.M., Brenna, M., Crase, J.A., Waight, T.E., van der Meer, Q.H.A., Cooper, A.F., Palin, J.M., Le Roux, P., and Münker, C., 2016, Peridotitic lithosphere metasomatized by volatile-bearing melts, and its association with intraplate alkaline HIMU-like magmatism: Journal of Petrology, v. 57, p. 2053–2078, https://doi.org/10.1093/petrology/egw069.
- Skemer, P., and Hansen, L.N., 2016, Inferring upper-mantle flow from seismic anisotropy: An experimental perspective: Tectonophysics, v. 668–669, p. 1–14, https://doi.org/10.1016/j.tecto.2015.12.003.
- Speciale, P.A., Behr, W.M., Hirth, G., and Tokle, L., 2020, Rates of olivine grain growth during dynamic recrystallization and postdeformation annealing: Journal of Geophysical Research: Solid Earth, v. 125, e2020JB020415, https://doi .org/10.1029/2020JB020415.
- Sutherland, R., Davey, F., and Beavan, J., 2000, Plate boundary deformation in South Island, New Zealand, is related to inherited lithospheric structure: Earth and Planetary Science Letters, v. 177,

- p. 141–151, https://doi.org/10.1016/S0012-821X(00)00043-1.
- Titus, S.J., Medaris, L.G., Wang, H.F., and Tikoff, B., 2007, Continuation of the San Andreas fault system into the upper mantle: Evidence from spinel peridotite xenoliths in the Coyote Lake basalt, central California: Tectonophysics, v. 429, p. 1–20, https://doi.org/10.1016/j.tecto.2006.07.004.
- Twiss, R.J., 1977, Theory and applicability of a recrystallized grain-size paleopiezometer: Pure and Applied Geophysics, v. 115, p. 227–244, https://doi.org/10.1007/BF01637105.
- Van der Wal, D., Chopra, P., Drury, M., and Fitz Gerald, J., 1993, Relationships between dynamically recrystallized grain size and deformation conditions in experimentally deformed olivine rocks: Geophysical Research Letters, v. 20, p. 1479–1482, https://doi.org/10.1029/93GL01382.
- Vauchez, A., Tommasi, A., and Mainprice, D., 2012, Faults (shear zones) in the Earth's mantle: Tectonophysics, v. 558–559, p. 1–27, https://doi .org/10.1016/j.tecto.2012.06.006.
- Vry, J.K., Baker, J., Maas, R., Little, T.A., Grapes, R., and Dixon, M., 2004, Zoned (Cretaceous and Cenozoic) garnet and the timing of high grade metamorphism, Southern Alps, New Zealand: Journal of Metamorphic Geology, v. 22, p. 137–157, https://doi.org/10.1111/j.1525-1314.2004.00504.x.
- Warren, J.M., and Hirth, G., 2006, Grain size sensitive deformation mechanisms in naturally deformed peridotites: Earth and Planetary Science Letters, v. 248, p. 438–450, https://doi.org/10.1016/j.epsl.2006.06.006.
- Zietlow, D.W., Sheehan, A.F., Molnar, P.H., Savage, M.K., Hirth, G., Collins, J.A., and Hager, B.H., 2014, Upper mantle seismic anisotropy at a strike-slip boundary: South Island, New Zealand: Journal of Geophysical Research: Solid Earth, v. 119, p. 1020–1040, https://doi.org/10.1002/2013JB010676.

Printed in USA